Journal of Solid State Chemistry 183 (2010) 736–743

Contents lists available at ScienceDirect

Journal of Solid State Chemistry

journal homepage: www.elsevier.com/locate/jssc

In situ generated dense shell-engaged Ostwald ripening: A facile controlled-preparation for $BaFe_{12}O_{19}$ hierarchical hollow fiber arrays

Fang-zhi Mou, Jian-guo Guan *, Zhi-gang Sun, Xi-an Fan, Guo-xiu Tong

State Key Laboratory of Advanced Technology for Materials Synthesis and Processing, Wuhan University of Technology, Wuhan 430070, PR China

ARTICLE INFO

Article history:
Received 29 September 2009
Received in revised form
14 January 2010
Accepted 16 January 2010
Available online 25 January 2010

Keywords:
Hollow fibers
Barrium ferrite
Electrospinning
Ostwald ripening
Hierarchical strcutures

ABSTRACT

This paper describes a simple and convenient approach to fabricate $BaFe_{12}O_{19}$ hierarchical hollow fibers or hollow fiber arrays by heat-treating electrospun solid fibers or fiber arrays using a deliberately devised two-step heat-treatment process, in which the dense shells generated in situ during the short-time pre-treatment procedure direct Ostwald ripening of flake-shaped $BaFe_{12}O_{19}$ nanocrystals in the elevated temperature heat-treatment procedure. The heat-treatment temperature has a strong effect on the structure and magnetic properties of the $BaFe_{12}O_{19}$ hierarchical hollow fibers and the resulting $BaFe_{12}O_{19}$ hierarchical hollow fiber arrays show a slight magnetic anisotropy as well as high coercivity. The in situ generated dense shell-engaged directing Ostwald ripening approach reported here can be readily extended to fabricate other metal oxides hollow fibers, and the resulting $BaFe_{12}O_{19}$ hierarchical hollow fibers or hollow fiber arrays are promised to have use in a number of applications that involve microwave absorber, magnetic separation, and so forth.

1. Introduction

The inorganic nanofiber and nanotube arrays with controlled morphology and crystallographics have great potential applications because of their unique structures [1,2]. At present, the template methods based on porous alumina or polymer membranes are widely used to synthesize oriented nanotube arrays, and various nanotube arrays, such as Fe [3], Ni [4], Co [5,6], Fe_2O_3 [7,8], $CoFe_2O_4$ [9], $ZnFe_2O_4$ [10], etc., are available. Obviously, the introduction of templates not only causes heterogeneous impurities but also increases manufacture cost. Electrospinning is another simple method for generating ultrathin inorganic solid and/or hollow fiber arrays with diameters ranging from tens of nanometers to tens of micrometers [11], and it has advantages of low cost, relatively high production rate and the applicability to many types of materials. In general, directly sintering electrospun gel fibers by the reported one-step heat treatment methods only produces solid fibers unless hollow electrospun gel fibers fabricated by a coaxial electrospinning technique are used as precursors. For example, metal nanofibers, such as Fe, Co and Ni nanofibers [12], and metal oxide nanofibers, such as CuO [13], TiO_2 [14] and MoO_3 [15] nanofibers, have been prepared by sintering the solid electrospun gel fibers. At the same time, TiO_2 [16], α-Fe_2O_3, γ-Fe_2O_3 and α-Fe [17] hollow fibers have also been successfully obtained by sintering hollow electrospun gel fibers, which were produced by the coaxial electrospinning technique. In this case, the inner and outer diameters of the hollow fibers strongly depend on the sizes of the coaxial, two-capillary spinneret. Therefore, to explore facile, template-free methods to prepare inorganic nanotube arrays is of practical significance.

Hexagonal barium ferrites ($BaFe_{12}O_{19}$), as an important magnetic material, exhibits high-coercivity, high-saturation magnetization, high electric resistance, low cost, excellent chemical stability and anticorrosion, and have been widely used in magnetic recording, microwave devices and electromagnetic shielding [18,19]. There are many reports pertaining to the synthesis of low-dimensional $BaFe_{12}O_{19}$, such as ultrafine powders [20], nanocrystals [21], hollow microspheres [22], nanoplates [23], and solid fibers [24]. To the best of our knowledge, $BaFe_{12}O_{19}$ hierarchical hollow fibers and hollow fiber arrays have not been reported so far. In this paper, we demonstrate a simple and convenient dense shell-engaged Ostwald ripening approach that allows for the facile fabrication of $BaFe_{12}O_{19}$ hierarchical hollow fibers or hollow fiber arrays using homogeneous electrospun gel solid fibers or fiber arrays as precursors. Different from the one-step heat treatment method reported in the previous literatures [11,24,25], the dense shell-engaged Ostwald ripening approach involves a deliberately devised two-step heat-treatment process, in which the dense shells generated in situ during the short-time pre-treatment procedure induce outward mass migration of small crystallites in the central part of fibers through

* Corresponding author. Fax: +86 27 87879468.
E-mail addresses: fanky_moe@yahoo.com.cn (F.Z. Mou), guanjg@whut.edu.cn (J.G. Guan), sun_zg@whut.edu.cn (Z.G. Sun), xafan@whut.edu.cn (X.A. Fan), wwhtgs@126.com (G.X. Tong).

0022-4596/$ - see front matter © 2010 Elsevier Inc. All rights reserved.
doi:10.1016/j.jssc.2010.01.016

Ostwald ripening mechanism during the subsequent high-temperature heat treatment procedure, forming hollow structures of the resultant fibers. The as-prepared $BaFe_{12}O_{19}$ hierarchical hollow fiber arrays exhibit slight magnetic anisotropies. The in situ generated dense shell-engaged Ostwald ripening approach reported here can be readily extended to fabricate other inorganic hollow structures, and the resulting $BaFe_{12}O_{19}$ hierarchical hollow fibers are expected to find use in fields of magnetic separation, microwave absorbers [19,26].

2. Experimental

All the raw materials used to synthesize $BaFe_{12}O_{19}$ hollow fibers were purchased from Sinopharm Chemical Reagent co., ltd, Shanghai, China. In a typical synthesis, into 30 mL of 0.1 g/mL iron citrate aqueous solution, stoichiometric $Ba(CH_3COO)_2 \cdot 2H_2O$ powders were firstly added according to a molar ratio of Fe^{3+} to Ba^{2+} of 12:1. Then, 2.49 g polyvinylpyrrolidone (PVP) with a molar weight of 50 000 was added into the above solution. Afterwards, the solution was stirred continuously at 60 °C until a precursor sol with a viscosity of 10 Pa s was available. The precursor sol was transferred into a syringe connected to a metallic nozzle, and fed at a constant rate of 0.3 mL/h through a syringe pump (TJ-1A, Longer Pump, China). In order to fabricate aligned fiber arrays, a copper frame was used as a collector, which was made up of parallel copper bars with a 5 mm gap between them. The metallic nozzle was connected to a high voltage supply (HB-Z303-20AC, Heng Bo High Voltage Power Supply Plant, China), and the collector was placed 10 cm below the metallic nozzle. Upon applying a high voltage of 25 kV, a fluid jet was ejected from the metallic nozzle. The solvent evaporated and the charged gel fiber was deposited on the collector, and aligned arrays of the electrospun fibers were obtained in the gaps. The collecting time of fiber arrays was about 5 min. All experiments were conducted at room temperature in air.

To obtain $BaFe_{12}O_{19}$ hierarchical hollow fiber arrays, the electrospun gel fiber arrays were firstly cut off by scissors and were then put into a porcelain boat. Afterwards, they were annealed in a tube furnace in air by a two-step heat-treatment process, which is described as follows: the electrospun gel fibers were firstly pre-treated in the air at an elevating temperature rate of 40 °C/min, and then were maintained at 400 °C for 30 min before cooled to room temperature. Secondly, the pre-treated electrospun gel fibers were heated to 150 °C at a heating rate of 5 °C/min, and then were held for 0.5 h before the temperature was increased to 450 °C at a heating rate of 0.5 °C/min, and were held at 450 °C for 4 h. Afterwards, the temperature was increased to 700 °C with a heating rate of 10 °C/min, and was maintained at 700 °C for another 4 h. $BaFe_{12}O_{19}$ hierarchical hollow fiber arrays were obtained after the fibers were naturally cooled to room temperature. In contrast, the $BaFe_{12}O_{19}$ hierarchical solid fiber arrays were also obtained by repeating the above heat treatment process but without the short time low-temperature pretreated procedure.

Scanning electron microscopy (SEM) images were obtained using a Hitachi S-4800 (Japan) Field-emission SEM. Transmission electron microscopy (TEM) image was captured on a JEM-100C (Japan) instrument at 100 kV. Thermogravity-differentiate scanning calorimeter (TG-DSC) analysis was carried out on a NETZSEC STA-449C (Germany) thermal analyzer. The phase purity of the products was examined by an X-ray diffraction (XRD) pattern obtained using a Rigaku D/max-IIIA (Japan) diffractometer at a voltage of 40 kV and a current of 200 mA with Cu$K\alpha$ radiation (λ=1.5406 Å), in the 2θ range from 10° to 90° at a scanning rate of 0.02° s^{-1}. The specific surface area was determined by a multipoint Brunauer–Emmett–Teller (BET) method using the adsorption data in the relative pressure (P/P_0) range of 0.05–0.25. Desorption isotherm was used to determine the pore size distribution using the Barret–Joymer–Halender method. The nitrogen adsorption volume at the relative pressure (P/P_0) of 0.970 was used to determine the pore volume and porosity. Magnetic properties of the samples were measured by a model 4HF vibrating sample magnetometer (VSM, ADE Co. Ltd, USA). To characterize magnetic anisotropic properties of the samples, the magnetization (M) and remnant magnetization (M_r) were measured as functions of the angle between the axis of oriented fibers and the applied magnetic field direction at room temperature and an applied field of 10 kOe.

3. Results and discussion

The preparation of aligned 1D magnetic nanostructures rather than randomly oriented configurations is of great interest for functional devices in nanoscale, especially for high-density information storage devices [27]. The aligned electrospun gel fibers can be easily obtained by employing a collector with gaps in it. Such a collector in our experiment was fabricated by putting several grounded copper bar in parallel arrangement with the gap of 5 mm. During the electrospinning process, the electrostatic force drives the positively charged fibers aligning between the two counter electrodes [28]. Fig. 1A shows the overall morphology of the as-prepared electrospun gel fiber arrays. The fibers are almost uniaxially aligned and have diameters of about 650 nm. The magnified image taken from the sections of the gel fibers (Fig. 1B) clearly indicates that the as-prepared gel fibers are solid in core.

Fig. 2A manifests that the resultant fibers obtained after annealing the gel fibers via the two-step heat treatment process have almost the same morphological features including the continuity and alignment as the electrospun precursor fibers shown in Fig. 1A. The SEM images of the sections and TEM image of the as-prepared fibers are shown in Fig. 2B and C, respectively. They clearly indicate that the solid gel fibers have been

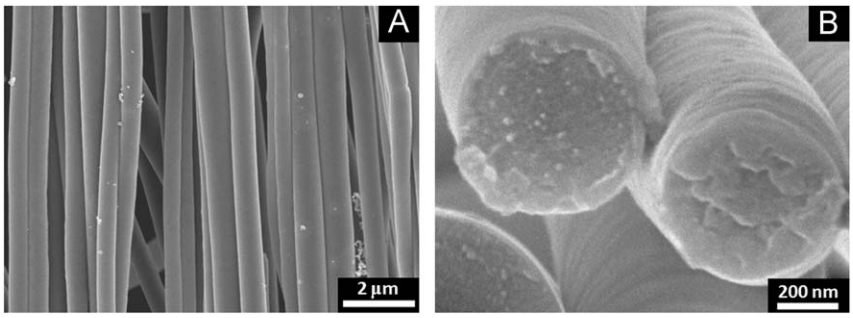

Fig. 1. SEM images of (A) the electrospun gel fiber arrays and (B) the sections.

transformed into the hollow structure after the two-step heat treatment process. The inner diameter and wall thickness of the as-prepared hollow fibers are ca. 250 and 80 nm, respectively. Compared with the gel fibers, the outer diameter of the hollow fibers decreases to about 410 nm. This is caused by the contraction as the organic components in the electrospun gel fibers will decompose and gasify during the heat treatment process. It is worth noting that the resultant fibers prepared by the two-step heat treatment process show a diameter shrinking rate of ca. 38.5%, which is much lower than that of the solid fibers obtained by the one-step heat treatment process (70–81% for Fe_2O_3, CoO and NiO [12], and 58% for $NiFe_2O_4$ [29] fibers). This phenomenon suggests that such a two-step heat treatment process hampers the electrospun gel fiber from the occurrence of center merge.

The crystalline structure of barium hexagonal ferrite ($BaFe_{12}O_{19}$) can be represented as a stacking of close-packed layers composed of larger oxygen and barium ions with smaller iron ions at the interstitial positions. Because of its anisotropic structure, $BaFe_{12}O_{19}$ will usually form particles with an anisotropic plate-like shape [30], and it is difficult to prepare $BaFe_{12}O_{19}$ with one-dimensional (1D) structure. Herein, the electrospun gel fiber is not only as a precursor, but also as the 1D template for the nucleation and growth of $BaFe_{12}O_{19}$ crystallites. As a result, the hierarchical fibers containing plate-like $BaFe_{12}O_{19}$ crystals form after the complete decomposition of organic components in the electrospun gel fiber. The inset of Fig. 2B, a magnified SEM image of the as-obtained fibers, indicates that the whole fiber consists of randomly oriented plate-like particles with 18 nm in thickness and about 50–150 nm in edge length. The hierarchical structure renders the fibers a rough surface with a large amount of irregular interspaces, which, in combination of the hollow structures, endows a relative high specific surface area and pore volume (Fig. S1). The XRD pattern of the as-obtained hollow fiber arrays is shown in Fig. 2D. All the peaks can be indexed as an M-type hexagonal structure except for the only slight peak at 33.15°, which corresponds to α-Fe_2O_3. The existence of α-Fe_2O_3 impurity suggests that the heat-treatment temperature (700 °C) is not high enough for α-Fe_2O_3 to completely transform into M-type hexagonal barium ferrites [31]. Unlike the oriented $BaFe_{12}O_{19}$ films [32], no preferential orientation is observed in the XRD pattern of the as-obtained $BaFe_{12}O_{19}$ hollow fiber arrays.

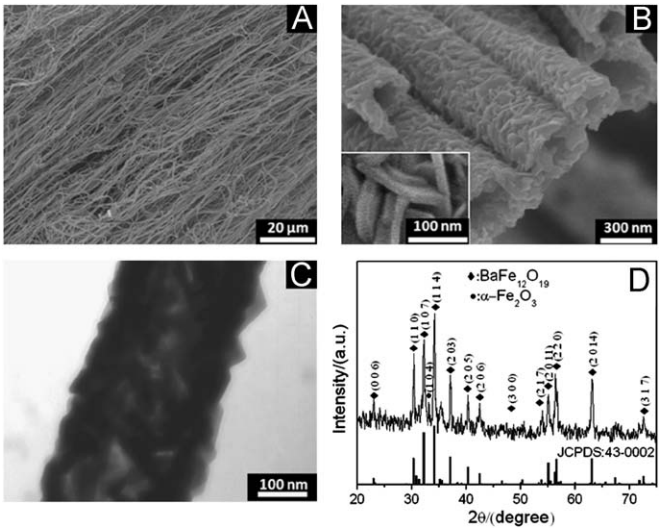

Fig. 2. SEM images of (A) the overall morphology; (B) the sections of the hierarchical $BaFe_{12}O_{19}$ hollow fiber arrays prepared by two-step treatment process, inset: the magnified morphology of the surface; (C) the TEM image taken from a typical hollow fiber; and (D) the XRD pattern of the as-obtained hollow fiber arrays.

It is known that directly annealing electrospun solid gel fibers at an elevated temperature by one-step heat treatment processes usually results in solid metal oxide fibers [24]. Fig. 3 depicts the SEM images of the $BaFe_{12}O_{19}$ fibers obtained at 700 °C for 4 h by the one-step treatment process without the pre-treatment procedure. As expected, similar to the samples prepared by the two-step heat-treatment process, the as-obtained $BaFe_{12}O_{19}$ fibers are almost uniaxially aligned along the longitudinal direction, and also consist of overlapped plate-like particles with about 18 nm in thickness, while they are solid in core with a diameter of about 350 nm (the inset of Fig. 3B). From this contrast experiment, it can be reasonably concluded that the pre-treatment procedure at 400 °C with an elevating temperature rate of 40 °C/min plays a key role in the formation of $BaFe_{12}O_{19}$ hollow fiber arrays as the major difference between these two methods is whether the short-time low-temperature rapid-heating pre-treatment procedure is introduced or not.

In order to understand the physical mechanism with regard to the influence of the pre-treatment procedure on the structure of resultant fibers, the intermediate products directly derived from the pre-treatment procedure were investigated. The SEM images of the fibers obtained from the pre-treatment procedure are shown in Fig. 4. Clearly, the obtained fibers have a uniform and smooth surface, and no plate-like nanoparticles are observed in their surfaces (Fig. 4A). Close examination of the cross section of the fiber seems to indicate that it shows a dense shell and loose core structure (Fig. 4B). To make a distinction between the dense shell and the loose core, a white circle is marked with an arrow in Fig. 4B. The formation of the loose core/dense shell structure may be reasonably attributed to the assumption that the outer part rather than the inner one of the electrospun precursor fibers can easily decompose and transform into inorganic matters (possibly a mixture of $BaCO_3$ and Fe_2O_3 [31]) during the short-time

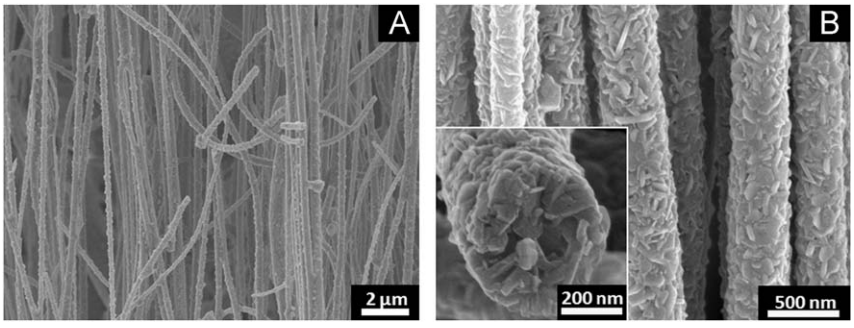

Fig. 3. SEM images of (A) the overall morphology, and (B) the magnified morphology of the hierarchical $BaFe_{12}O_{19}$ fiber arrays prepared by the one-step treatment process at 700 °C for 4 h, inset: the section of a typical $BaFe_{12}O_{19}$ solid fiber.

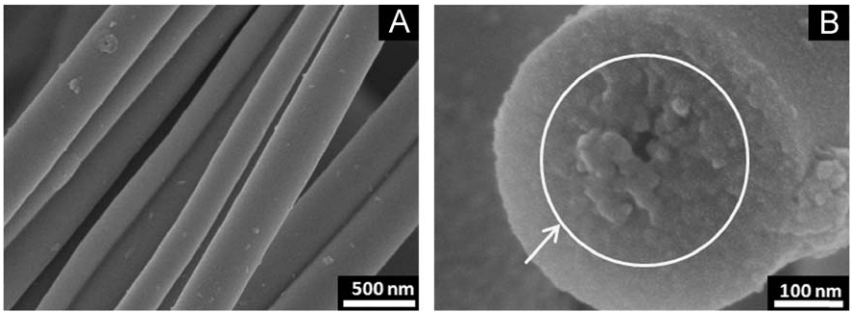

Fig. 4. SEM images of (A) the fiber arrays obtained from pre-treatment at 400 °C for 30 min, and (B) the section of a typical pre-treated fiber.

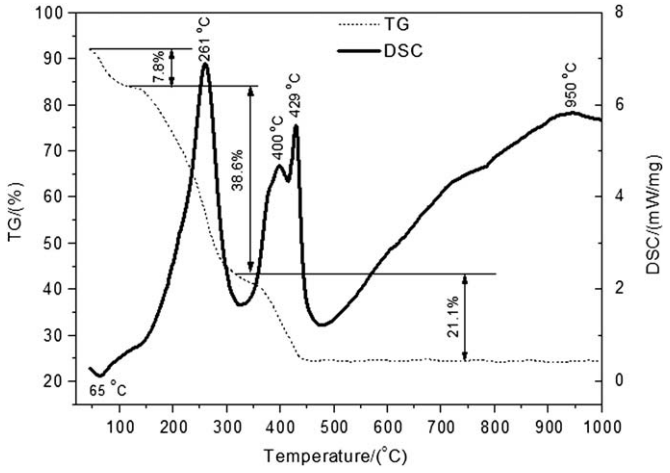

Fig. 5. TG-DSC analysis for the electrospun gel fibers.

rapid-heating pre-treatment procedure. As the elevating temperature rate of 40 °C/min in the short time pre-treatment procedure is high enough to engender a remarkable temperature gradient along the radial direction, this will lead to the formation of dense rigid inorganic shells consisting of $BaCO_3$ and Fe_2O_3 in the surface and a small void in the central part of the gel fibers. As a result, a dense shell/loose core structure is created after the electrospun gel fibers were pre-treated at 400 °C for 30 min (Fig. 4). To further confirm this, we have carried out the TG-DSC analysis of the electrospun precursor fibers. As shown in Fig. 5, the electrospun precursor fibers have three differentiated steps of weight loss in the temperature range of 40–1000 °C. The first weight loss occurs at around 40–150 °C, accompanied with a broad endothermic peak at 65 °C. This can be ascribed to the evaporation of water. The second weight loss of 38.6% appears at around 150–315 °C, corresponding to a sharp exothermic peak at about 265 °C. This may be attributed to the decomposition of organic salts including iron citrate and barium acetate along with the degradation of PVP through the intermolecular cross-linking reaction [33,34]. The third step at around 315–450 °C involves 21.1% weight loss and accompanies two sharp exothermic peaks at 400 and 429 °C in the DSC curve, which could be attributed to the oxidation of carbon released by the decomposition of PVP [34]. At temperature higher than 450 °C, no weight loss is observed in the TG curve. This indicates that the organic components have completely decomposed before 450 °C. The strong broad exothermic peak in the range of 480–1000 °C is ascribed to the growth of $BaFe_{12}O_{19}$ crystallites. Obviously, the short-time pre-treatment temperature of 400 °C is reasonably supposed to be high enough to form a dense shell the electrospun precursor fibers, while it is close to the temperature at which iron citrate transforms into α-Fe_2O_3 [17], and lower than the formation temperature of $BaFe_{12}O_{19}$. Thus, an appropriate amount of residual organic components can be sustained in the electrospun precursor fibers to prevent the precipitation of α-Fe_2O_3 particles, which is harmful for the formation of $BaFe_{12}O_{19}$ [31].

Based on the above experimental results, we propose an underlying mechanism for the formation of the as-obtained $BaFe_{12}O_{19}$ hollow fibers that involves an in situ generated dense shell inducing oriented Ostwald ripening. Generally, Ostwald ripening involves the initial formation of small crystals and the subsequent growth of bigger crystals at the expense of smaller crystals due to the energy difference among them [35,36]. Consequently, when the larger crystals grow, the area around them is depleted of smaller crystals. In our protocol, the electrospun precursor fibers are uniform in radial direction and have a smooth surface, as shown in Fig. 1. When they are pretreated with a high heating rate of 40 °C/min at 400 °C for 30 min, a loose core/dense shell structure is formed (Fig. 4). In the pre-treated electrospun precursor fibers with this peculiar core/shell structure, metallic ions show a decreasing concentration gradient from its surface to the center. When they are applied by the high-temperature heat treatment, $BaFe_{12}O_{19}$ crystals would favorably be formed in the outer part prior to in the inner one. In other words, the $BaFe_{12}O_{19}$ crystals formed in the outer shell are statistically bigger than those in the inner part. Thus, during the high-temperature heat treatment procedure, the larger crystals in the outer part of the fibers are essentially immobile while the smaller crystals in the central part undergo an oriented mass transfer to the outer shell by a recrystallization process, because the latter show higher surface energies and less stable than the former. As a result, an interior space is created within the fibers and hollow tubular structures are available (Fig. 2). To this extent, the dense shell of the pre-treated fibers can be regarded as a framework to prevent the $BaFe_{12}O_{19}$ crystals formed by the high-temperature heat treatment from growing and aggregating in the inner core. With the Ostwald ripening time prolonging, smaller crystals located in the inner part of the fibers will continue to be devoured by the larger crystals in the outer shell, resulting in the continued expansion of interior space and growth of the plate-like $BaFe_{12}O_{19}$ crystals constituting the hierarchical hollow fibers. The formation process of $BaFe_{12}O_{19}$ hollow fibers is illustrated in Fig. 6A. When the electrospun precursor fibers are applied directly by the one-step high temperature heat-treatment process without the pre-treatment, $BaFe_{12}O_{19}$ crystals will form and grow simultaneously in the core and surface of the precursor fibers. Hence, the smaller crystals act as "nutrients" for the bigger crystals randomly distributed in the fibers during the heat treatment process, and the final products tend to be porous solid fibers (Fig. 6B). The formation of the as-obtained solid $BaFe_{12}O_{19}$ fibers by one-step heat treatment was also reported by Guo [24].

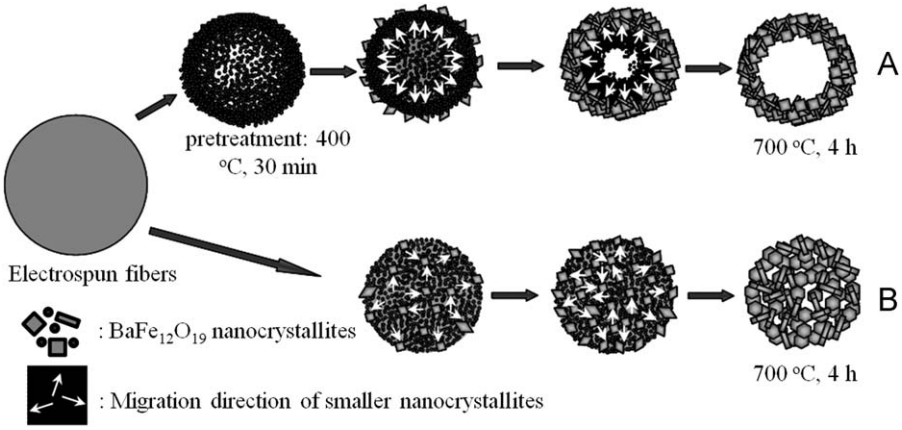

Fig. 6. Schematic diagram of structural transformation of the section of (A) hollow fibers and (B) solid fibers during the heat treatment process.

To further substantiate the proposed formation mechanism of the $BaFe_{12}O_{19}$ hierarchical hollow fibers, the influences of the annealing temperature (T) of the high-temperature annealing procedure on the morphology and crystalline structure of $BaFe_{12}O_{19}$ fibers are also investigated. When the pre-treated fibers are annealed at 500 °C for 4 h, the resultant fibers consisting of nanoparticles show a smooth surface with a few plate-like nanoparticles sprinkling on it (Fig. 7A). This confirms that relative larger plate-like nanoparticles are initially generated in the surface of fibers. The inset of Fig. 7A indicates that the fibers maintain the initial loose core/dense shell structure and the tubular structures are not still obtained at this stage. With T increasing to 700 °C, the as-obtained fibers have a hollow tubular structure with much rougher surfaces, and the whole fibers are composed of $BaFe_{12}O_{19}$ nanoplates of about 18 nm in thickness (Fig. 7B). This validates that the hollow fibers are formed via the growth of $BaFe_{12}O_{19}$ crystals through an Ostwald ripening mechanism. Further increasing T to 800 °C increases the size of the $BaFe_{12}O_{19}$ nanoplates and decreases the hollow interior space of the resultant fibers. As shown in Fig. 7C, the hollow tubular fibers obtained at 800 °C consists of the $BaFe_{12}O_{19}$ nanoplates of about 20 and 200 nm in the thickness and edge length, respectively, and the hollow structure of about 180 nm in diameter. Fig. 7D manifests that for the hollow fibers obtained at 1000 °C, the thickness and edge length of the $BaFe_{12}O_{19}$ nanoplates sharply increase to about 55 and 280 nm, respectively, and the hollow structure further shrinks to about 150 nm. Close examination of Fig. 7B to D indicates that the fibers obtained at 700 °C have a relative denser surface than those obtained at 800 or 1000 °C. The former consist of large $BaFe_{12}O_{19}$ nanoplates with small nanoparticles filling in the interspaces between them. For the latter, the small nanoparticles vanish, instead cavities form, and the size of these cavities increases with increasing the annealing temperature. The XRD patterns of the fibers obtained at different annealing temperatures are shown in Fig. 7E. It can be seen that the fibers obtained at 500 °C show no obvious peak in its XRD pattern and are an amorphous matters. The M-type hexagonal $BaFe_{12}O_{19}$ fibers are formed at 700 °C, while a small amount of α-Fe_2O_3 impurity still exists in the samples. All the XRD peaks for the samples obtained at 800 and 1000 °C can be indexed as the M-type hexagonal structure and no impurity phases are detected. Compared to the fibers obtained at 700 °C, those obtained at 800 and 1000 °C show an enhanced intensity of XRD peaks, indicating the improved crystallization of $BaFe_{12}O_{19}$ fibers. Obviously, the above results support our proposal that the $BaFe_{12}O_{19}$ hollow fibers are generated via an oriented Ostwald ripening induced by an in situ generated dense shell, which is obtained by a short-time low-temperature rapid-heating pre-treatment procedure.

It is well known that the arrays of solid or hollow fibers usually exhibit a distinctive anisotropic magnetic property compared with the unassembled magnetic nanomaterials [4–10]. In order to investigate magnetic anisotropic property of the $BaFe_{12}O_{19}$ hollow fiber arrays prepared at 700 °C, hysteresis loops with field parallel ($\parallel$) and perpendicular ($\perp$) to the hollow fibers' long axis were measured at room temperature, as shown in Fig. 8A. The samples along the two directions both show high coercivity (H_c) values of about 4300 Oe without any discernible differences. However, the saturated magnetization (M_s) and M_r along the parallel direction are a little higher than those along the perpendicular direction. This suggests that the easy axis lies along the fibers axis. Additional evidence for magnetic anisotropies of the as-prepared hollow fiber arrays is provided by the dependence of M and M_r on the angle between the direction of the applied magnetic field and that of the hollow fibers' long axis (θ) measured at the room temperature at the applied field of 10 kOe, as shown in Fig. 8B and C. It can be seen that M/θ and M_r/θ curves show a bell-shaped behavior, that is, both M and M_r reach maximal values at θ=0°. The varying rate $\Delta M/M_0$ and $\Delta M_r/M_{r0}$ can reach as high as 13.3% and 16.2% as θ increases from 0° to 90°, here M_0 and M_{r0} are the magnetization and remanence measured at 0°, $\Delta M = M_0 - M_{90}$ and $\Delta M_r = M_{r0} - M_{r90}$. These results indicate that the as-prepared $BaFe_{12}O_{19}$ hollow fiber arrays only have a slight magnetic anisotropy due to the $BaFe_{12}O_{19}$ nanoplatelets which are almost randomly oriented in the hollow fibers. The similar slight magnetic anisotropy has also been observed in the arrays of polycrystalline iron nanorods consisting of randomly oriented Fe grains [37].

One-dimensional ferromagnetic materials generally yield to a nonsquare hysteresis loop when the magnetic field is perpendicular to the fiber axis, as the demagnetizing factor is up to 2π in this case [37]. However, the as-prepared hollow fiber arrays do not show such a behavior. Instead, the loop shapes are similar for both parallel and perpendicular directions. This may also be attributed to the very weak preferential orientation of the plate-like grains in the hollow fibers, as confirmed by the SEM and XRD analysis.

The room temperature magnetic properties of the $BaFe_{12}O_{19}$ hollow fibers prepared at 700, 800 and 1000 °C are shown in Fig. 8D. It can be seen that the double-S shaped hysteresis loop is observed for the $BaFe_{12}O_{19}$ hollow fibers obtained at 700 °C,

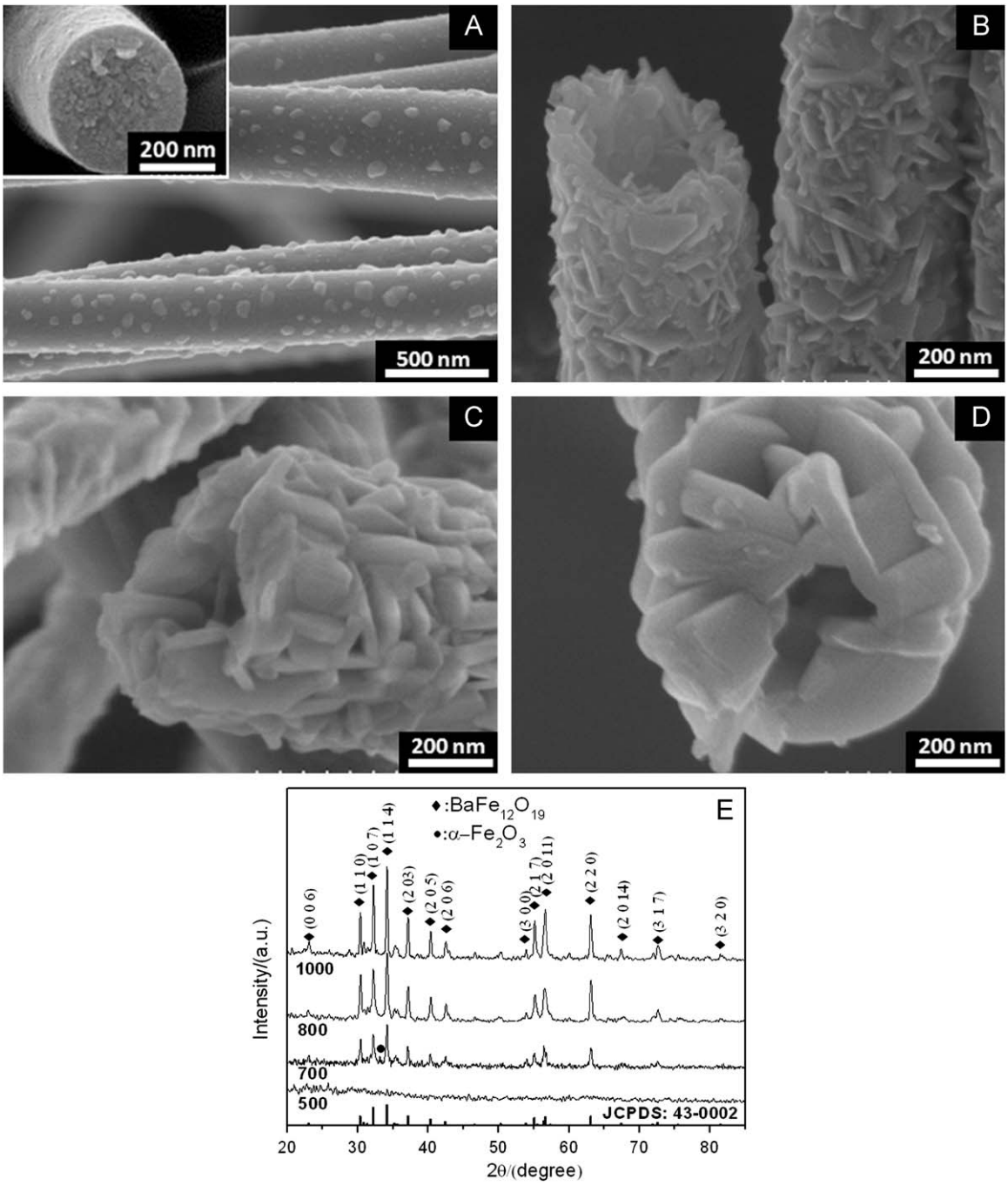

Fig. 7. SEM images of the fibers obtained after the subsequent heat treatment process at (A) 500, (B) 700, (C) 800 and (D) 1000 °C, respectively; and (E) the XRD patterns of the as-obtained fibers. The inset in A shows the typical section of the fibers obtained after the subsequent heat treatment process at 500 °C.

which is typical for the material composed of two magnetic phases. Fig. 8E shows that when temperature increases from 290 to 770 K, the magnetization initially decreases, then increases to a maximum before abruptly decreases. This indicates that the $BaFe_{12}O_{19}$ hollow fibers obtained at 700 °C exhibit obvious Hopkinson effect, revealing the single domain characteristics of the barium hexaferrite particles [38,39]. The Curie temperature (T_c) is observed to be about 730 K, while the magnetization above T_c does not decrease to zero, suggesting that the secondary magnetic phase of maghemite (γ-Fe_2O_3) exists in the samples as the T_c of γ-Fe_2O_3 is 948 K [40], higher than that of $BaFe_{12}O_{19}$. This phenomenon is also observed in the $BaFe_{12}O_{19}$ nanoparticles obtained by sintering the citrate precursors at 650–750 °C [31]. Due to the overlapping of the γ-Fe_2O_3 and $BaFe_{12}O_{19}$ XRD peaks, the γ-Fe_2O_3 impurity is not detected in Fig. 7E. In contrast, the α-Fe_2O_3 impurity, which is detected by XRD, has a negligible influence on the hysteresis loop and the thermomagnetization of the samples [41]. Hence, the double-S shaped hysteresis loop for the $BaFe_{12}O_{19}$ hollow fibers obtained at 700 °C is reasonably attributed to the small amount of γ-Fe_2O_3 impurity. The double-S shaped hysteresis loop is disappeared when the T is elevated to 800 and 1000 °C, suggesting the availability of a single phase $BaFe_{12}O_{19}$. This is consistent with the XRD analysis of Fig. 7E. The M_s of the $BaFe_{12}O_{19}$ hollow fibers slightly increases from 46.15, 47.39 to 51.56 emu/g, and M_r also increases from 22.54, 26.34 and 27.59 emu/g when T increases from 700 to 800 and 1000 °C. This

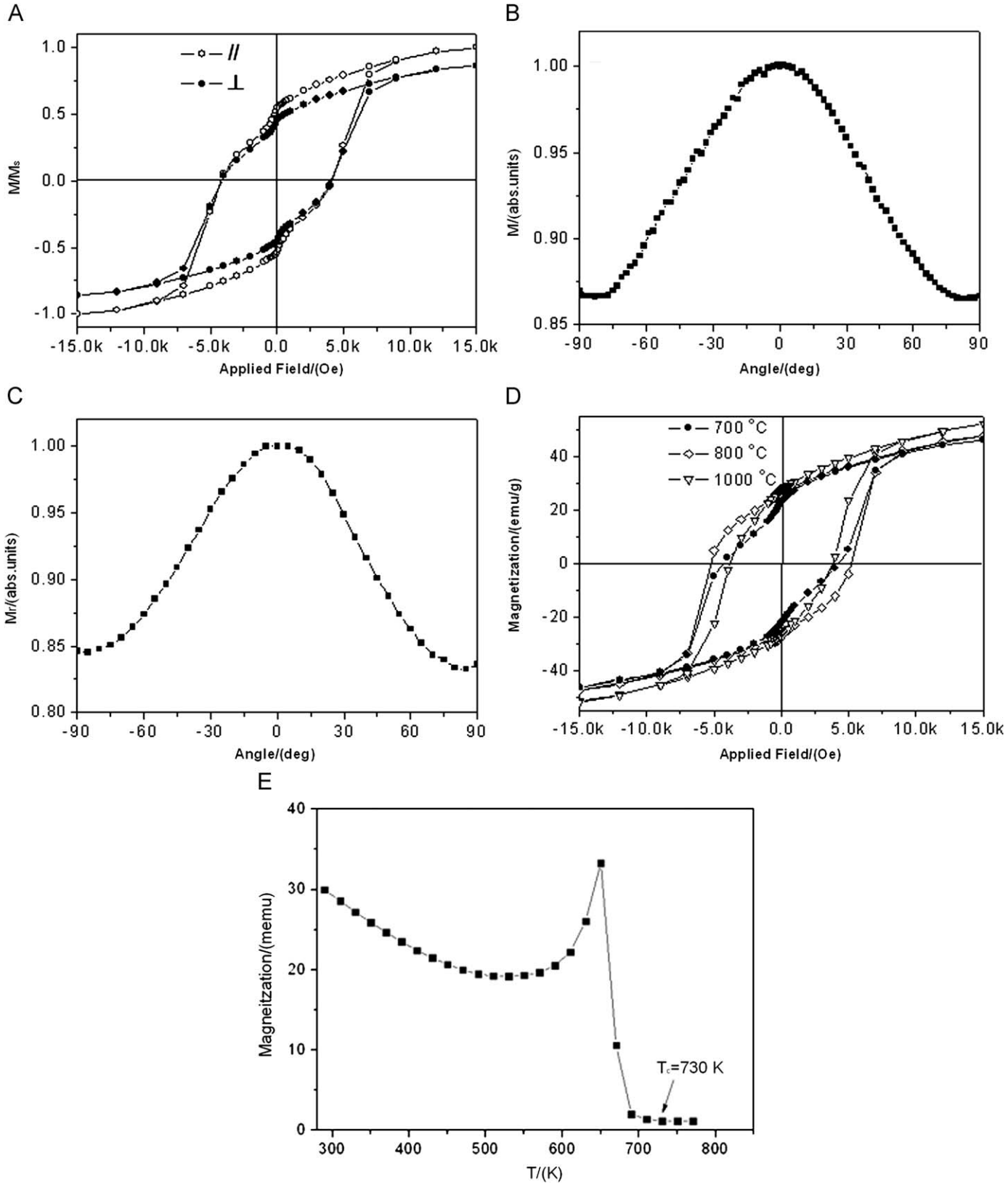

Fig. 8. (A) the room temperature magnetic hysteresis loops measured parallelly (∥) and perpendicularly (⊥) to the long axis of $BaFe_{12}O_{19}$ hollow fibers; the angular dependence of (B) magnetization and (C) remanence curves of the $BaFe_{12}O_{19}$ hollow fiber arrays prepared at 700 °C at the applied field of 10 kOe; (D) the room temperature hysteresis loops for the fibers prepared at 700, 800 and 1000 °C, respectively; and (E) the thermomagnetization analysis of $BaFe_{12}O_{19}$ hollow fibers prepared at 700 °C at the applied field of 1 kOe.

may be attributed to the improvement of the purity and crystallinity of $BaFe_{12}O_{19}$ crystallites according to the XRD analysis (Fig. 7E), as well as the shrinkage of the surface effects with increasing T [42]. The M_s of the as-obtained $BaFe_{12}O_{19}$ hollow fibers is below the theoretical value (72 emu/g) [43], but is comparable to that of the reported $BaFe_{12}O_{19}$ hollow microspheres [22], nanoplates [23], nanoparticles [44], and nanospheres [45]. This may be explained by the surface spin-canting phenomenon, purity and particle size effects [46]. Fig. 8D also shows that when T increases from 700 to 800 and 1000 °C, the H_c of the as-obtained $BaFe_{12}O_{19}$ hierarchical hollow fibers firstly increases, then decreases. Similar phenomenon is also reported and explained in terms of the crystallinity, grain size and magnetic domain structure by the literatures [22,47]. The maximal H_c reaches as big as 5226 Oe and is larger than that of the $BaFe_{12}O_{19}$ nanoplates (910 [48] and 1200 Oe [23]) and hollow spheres (3400–3200 Oe) [22]. This suggests that they have potential applications in microwave absorbers, magnetic separation, and so forth. All these results clearly demonstrate that annealing temperature have a remarkable influences of the magnetic property of the as-obtained $BaFe_{12}O_{19}$ hierarchical tubular fibers.

4. Conclusion

In summary, we demonstrate a simple fabrication of $BaFe_{12}O_{19}$ hierarchical hollow fibers or their arrays by a dense shell-engaged Ostwald ripening approach using electrospun gel solid fibers or fiber arrays as precursors without using any solid templates. The hollow structure of $BaFe_{12}O_{19}$ hierarchical hollow fibers can be achieved by a deliberately devised two-step heat-treatment process, in which the dense shells generated in situ during the short-time pre-treatment procedure direct Ostwald ripening of flake-shaped $BaFe_{12}O_{19}$ crystals in the elevated temperature heat-treatment procedure. The heat-treatment temperature has a great influence on the structure including the hollow size and shell thickness, etc. and magnetic properties of the $BaFe_{12}O_{19}$ hierarchical hollow fibers. We believe that the two-step dense shell-engaged directing Ostwald ripening approach reported here can be readily extended to fabricate other metal oxides one-dimensional hollow fibers. Due to the big specific surface area and high coercivity, the resulting $BaFe_{12}O_{19}$ hierarchical hollow fibers and the hierarchical hollow fiber arrays are expected to find use in a number of applications that involve microwave absorbers, magnetic separation, and so forth.

Acknowledgments

This work was supported by National high-technology Research and Development Program of China (no. 2006AA03A209), National Basic Science and Research Project (D1420061057), Young Teachers from Fok Ying Tung Education Foundation (no. 101049), New Century Excellent Talents (no. NCET-05-0660) from the Ministry of Education, and China Postdoctoral Science Foundation (no. 20070420169).

Appendix A. Supplementary material

Supplementary data associated with this article can be found in the online version at doi:10.1016/j.jssc.2010.01.016.

References

[1] Z.R.R. Tian, J.A. Voigt, J. Liu, B. McKenzie, M.J. McDermott, M.A. Rodriguez, H. Konishi, H.F. Xu, Nat. Mater. 2 (2003) 821.
[2] D. Wang, F. Qian, C. Yang, Z.H. Zhong, C.M. Lieber, Nano Lett. 4 (2004) 871.
[3] D. Borissov, S.I. Uppenkamp, M. Rohwerder, J. Phys. Chem. C 113 (2009) 3133.
[4] X.M. Wang, Z.H. Yuan, S.Q. Sun, Y.Q. Duan, L.J. Bie, Mater. Chem. Phys. 112 (2008) 329.
[5] T.N. Narayanan, M.M. Shaijumon, P.M. Ajayan, M.R. Anantharaman, J. Phys. Chem. C 112 (2008) 14281.
[6] D.D. Li, R.S. Thompson, G. Bergmann, J.G. Lu, Adv. Mater. 20 (2008) 4575.
[7] H.J. Zhou, S.S. Wong, ACS Nano 2 (2008) 944.
[8] X.L. Yu, C.B. Cao, X.Q. An, Chem. Mater. 20 (2008) 1936.
[9] Y. Xu, J. Wei, J.L. Yao, J.L. Fu, D.S. Xue, Mater. Lett. 62 (2008) 1403.
[10] F.F. Liu, X.Y. Li, Q.D. Zhao, Y. Hou, X. Quan, G.H. Chen, Acta Mater. 57 (2009) 2684.
[11] D. Li, J.T. McCann, Y.N. Xia, J. Am. Ceram. Soc. 89 (2006) 1861.
[12] H. Wu, R. Zhang, X.X. Liu, D.D. Lin, W. Pan, Chem. Mater. 19 (2007) 3506.
[13] H. Wu, D. Lin, W. Pan, Appl. Phys. Lett. 89 (2006) 133125.
[14] D. Li, Y.L. Wang, Y.N. Xia, Nano Lett. 3 (2003) 1167.
[15] S.Z. Li, C.L. Shao, Y.C. Liu, S.S. Tang, R.X. Mu, J. Phys. Chem. Solids 67 (2006) 1869.
[16] D. Li, Y.N. Xia, Nano Lett. 4 (2004) 933.
[17] S.H. Zhan, D.R. Chen, X.L. Jiao, S.S. Liu, J. Colloid Interface Sci. 308 (2007) 265.
[18] G.Z. Shen, M. Xu, Z. Xu, Mater. Chem. Phys. 105 (2007) 268.
[19] R. Sharma, R.C. Agarwala, V. Agarwala, Mater. Lett. 62 (2008) 2233.
[20] L.X. Wang, Q.T. Zhang, J. Alloys Compd. 454 (2008) 410.
[21] E. Paimozd, A. Ghasemi, A. Jafari, H. Sheikh, J. Magn. Magn. Mater. 320 (2008) L137.
[22] P. Ren, J.G. Guan, X.D. Cheng, Mater. Chem. Phys. 98 (2006) 90.
[23] D. Miha, K. Matjaz, Z. Andrei, H. Darko, L. Darja, J. Am. Ceram. Soc. 90 (2007) 2057.
[24] Y.Z. Guo, C.J. Li, J.N. Wang, Chin. J. Inorg. Chem. 25 (2009) 1018.
[25] M. Graeser, M. Bognitzki, W. Massa, C. Pietzonka, A. Greiner, J.H. Wendorff, Adv. Mater. 19 (2007) 4244.
[26] J.H. Nam, Y.H. Joo, J.H. Lee, J.H. Chang, J.H. Cho, M.P. Chun, B.I. Kim, J. Magn. Magn. Mater. 321 (2009) 1389.
[27] H. Masuda, K. Fukuda, Science 268 (1995) 1466.
[28] D. Li, Y.N. Xia, Adv. Mater. 16 (2004) 1151.
[29] D. Li, T. Herricks, Y.N. Xia, Appl. Phys. Lett. 83 (2003) 4586.
[30] E. Pollert, Prog. Cryst. Growth Charact. 11 (1985) 155.
[31] W. Zhong, W.P. Ding, Y.M. Jiang, N. Zhang, J.R. Zhang, Y.W. Du, Q.J. Yan, J. Am. Ceram. Soc. 80 (1997) 3258.
[32] X.H. Liu, M.H. Hong, W.D. Song, G.X. Chen, J.F. Chong, J.P. Wang, Y.H. Wu, T.C. Chong, Appl. Phys. A 78 (2004) 423.
[33] P.M. Remiro, M.M. Cortazar, M.E. Calahorra, J. Mater. Sci. 34 (1999) 2627.
[34] Z.L. Wang, X.J. Liu, M.F. Lv, P. Chai, Y. Liu, J. Meng, J. Phys. Chem. B 112 (2008) 11292.
[35] H.G. Yang, H.C. Zeng, J. Phys. Chem. B 108 (2004) 3492.
[36] H.C. Zeng, Curr. Nanosci. 3 (2007) 177.
[37] L. Vayssieres, L. Rabenberg, A. Manthiram, Nano Lett. 2 (2002) 1393.
[38] O. Popov, P. Racher, M. Mikkov, F. Calderon, J.L. Sanchez Ll, F. Leccabue, J. Magn. Magn. Mater. 99 (1991) 119.
[39] C. Sudakar, G.N. Subbanna, T.R.N. Kutty, J. Magn. Magn. Mater. 263 (2003) 253.
[40] R.M. Bozorth, Ferromagnetism, D. Van Nostrand, New York, 1950.
[41] D. Lisjak, K. Bobzin, K. Richardt, M. Bégard, G. Bolelli, L. Lusvarghi, A. Hujanen, P. Lintunen, M. Pasquale, E. Olivetti, M. Drofenik, T. Schläfer, J. Eur. Ceram. Soc. 29 (2009) 2333.
[42] G.F. Goya, T.S. Berquo, F.C. Fonseca, M.P. Morales, J. Appl. Phys. 94 (2003) 3520.
[43] B.T. Shirk, W.R. Buessem, J. Appl. Phys. 40 (1969) 1294.
[44] M.H. Kim, D.S. Jung, Y.C. Kang, J.H. Choi, Ceram. Int. 35 (2009) 1933.
[45] H.M. Lee, S.Y. Bae, J.H. Yu, Y.J. Kim, J. Am. Ceram. Soc. 91 (2008) 2856.
[46] K.V.P.M. Shafi, Y. Koltipin, A. Gedanken, R. Prozorov, J. Balogh, J. Lendvai, I.J. Felner, J. Phys. Chem. B 101 (1997) 6409.
[47] J.H. Dho, E.K. Lee, J.Y. Park, N.H. Hur, J. Magn. Magn. Mater. 285 (2005) 164.
[48] T. Yamauchi, Y. Tsukahara, T. Sakata, H. Mori, T. Chikata, S. Katoh, Y. Wad, J. Magn. Magn. Mater. 321 (2009) 8.